RSC Advances

PAPER

View Article Online
View Journal | View Issue

Check for updates

Cite this: *RSC Adv.*, 2018, **8**, 38410

Luminescent properties of Eu-doped magnetic Na_3FeF_6†

Hong Jia,[a] Yiping Zhou,[a] Xiaoyan Wang,[a] Weiying Zhang,*[a] Xun Feng,[a] Zhiang Li,[a] Hongzhi Fu,[a] Jianguo Zhao,*[a] Zhongli Liu*[a] and Xiaofeng Liu[b]

Received 27th August 2018
Accepted 8th November 2018

DOI: 10.1039/c8ra07137c

rsc.li/rsc-advances

Sodium iron fluoride (Na_3FeF_6) is a colorless ferromagnetic fluoride with a monoclinic crystal structure (space group *P*21/*c*), and it is expected to be an ideal platform for exploring magneto-optical interactions. In the present work, Eu^{3+} doped Na_3FeF_6 micro-powders were synthesized by a hydrothermal method, and the structures were examined by X-ray diffraction (XRD) and scanning electron microscopy (SEM). The optical properties were examined using UV-Vis spectra and fluorescence spectra, and the results show that the emission spectra can be finely tuned by the hydrothermal reaction temperature and doping concentration of Eu ions. We found that Na_3FeF_6 doped with 5% Eu^{3+} synthesized at 196 °C exhibited the optimal red emission under excitation at 395 nm. The magnetization of Na_3FeF_6:5% Eu^{3+} decreased rapidly from about 7.85 emu g^{-1} at 5 K to 0.4 emu g^{-1} at 60 K, then slowly decreased with temperature increase from 60 K to 300 K. This Eu^{3+} doped Na_3FeF_6 powder is expected to find potential applications in the field of magneto-optical modulation and relevant devices.

1. Introduction

Due to the applications in biomedical imaging, cancer therapy and sensing, magneto-optical bi-functional nanomaterials have attracted growing attention in the past decade.[1–3] Magnetic nanomaterials such as superparamagnetic nanocrystals can be used as drug carriers and magnetic resonance imaging materials in the bio-medicine field. The introduction of optical functionality to these magnetic nanocrystals could greatly extend their application in diverse fields. For example, the magneto-optical hybrid nanoparticles formed by the combination of upconversion nanoparticles and magnetic Fe_3O_4 nanoparticles can be used both as drug carriers and as nanoscale magneto-optical nanoprobes.[4–10]

In recent years, the research of magneto-optical bi-functional nanomaterials mostly focuses on the combination of magnetic and optical properties in a single particle, such as rare-earth (RE) doped materials.[11–15] The matrix of these magneto-optical materials is mostly not magnetic or only paramagnetic. Therefore, the study of the magneto-optical effect, especially the interaction between magnetism and photoluminescence, requires the use of strong magnetic field. The introduction of strong (ferromagnetic) magnetic materials can only be realized through the fabrication of core–shell structure, such as the $Fe_3O_4@Y_2O_3$:Eu.[16] However, most ferromagnetic materials including Fe_3O_4 strongly absorbs visible light and quenches the emission of the RE ions.[17–23] Therefore, the search of a colorless magnetic host could be of great interest for the investigation of the magneto-optical effect.

Sodium iron fluoride (Na_3FeF_6) is a colorless, ferromagnetic fluoride, and it is an ideal platform for the exploration of magneto-optical interactions.[24–26] In this work, Na_3FeF_6 doped with Eu^{3+} ions were prepared by hydrothermal method. The Na_3FeF_6:Eu powders were characterized with X-ray diffraction (XRD), scanning electron microscopy (SEM). Under excitation by UV light, visible emission can be observed from the Na_3FeF_6:Eu, and luminescence intensity from Na_3FeF_6:Eu were optimized by adjusting different reaction temperature and doping concentration of Eu ions. This Na_3FeF_6:Eu phosphors might be explored as a magneto-optical dual-functional material.

2. Experimental

2.1 Sample synthesis

The powders of $Fe(NO_3)_3$, NaF, and NH_4HF_2 were dissolved in deionized water respectively to get a concentration of 0.1mol l^{-1} $Fe(NO_3)_3$, 0.5 mol l^{-1} NaF and 0.5mol l^{-1} NH_4HF_2 for each solutions. These solutions were mixed with a volume ratio of v$[Fe(NO_3)_3]$: v[NaF] : v$[NH_4HF_2]$ = 1 : 1 : 3, and then 3 ml HF were added into the mixed solutions (75 ml). Finally, 0.1 mol l^{-1}

[a]College of Physics and Electronic Information & Henan Key Laboratory of Electromagnetic Transformation and Detection, Luoyang Normal University, Luoyang 471934, China. E-mail: jiahong517@aliyun.com

[b]School of Materials Science and Engineering, Zhejiang University, Hangzhou 310027, China

† Electronic supplementary information (ESI) available. See DOI: 10.1039/c8ra07137c

$Eu(NO_3)_3$ was added to the above solution with the volume ratio of v[Eu] : v[Fe] = 3%, 5%, 7%, 10%, 15%, 18%. The mixed solution was transferred into an autoclave, and then heated at 196 °C for 16 hours. After cooling to room temperature, the products were collected from the resultant solutions by centrifugation at 8000 rpm for 20 min. The obtained phosphor powders were washed for three times and then dried at 60 °C.

2.2 Characterizations

The crystal structures of all the samples were studied by X-ray diffraction (XRD) with a RIGAKU D/MAX 2550/PC system operated at a step size of 0.02° at a scanning speed of 5° min^{-1} using Cu Kα radiation ($\lambda = 1.5406$ Å). Scanning electron microscope (SEM) images were taken using a Hitachi S-4800 scanning electron microscope. The UV-Vis spectra diffuse reflectance spectra of the films were measured at room temperature on a UV-3600 Plus spectrophotometer. The luminescence spectra of the samples were investigated using a Japan F-4600 fluorescence spectrophotometer. Magnetic properties were performed on a Quantum Design SQUID MPMS XL-7 (SQUID).

3. Results and discussion

3.1 Structure of the Na_3FeF_6

Fig. 1a shows the crystal structure of Na_3FeF_6 projected along the *a*-axis. The structure of Na_3FeF_6 is isomorphic with cryolyte-like structures (K_2NaScF_6, Na_3CrF_6 and Na_3AlF_6) with the monoclinic symmetry that belongs to the space group *P*21/*c*.[27,28] There are three sodium sites, namely the Na1 site that is located at the distorted octahedral site of NaF_6, the Na2 site at the bipyramidal site of (NaF_5), and finally the Na3 site at the distorted tetrahedral site of NaF_4 (Fig. 1(b)). All the Fe atoms are located at the distorted FeF_6 octahedral sites. Furthermore, it can be observed that Na1 octahedral sites and Na3 tetrahedral sites actually share corner sites. Na1 octahedral sites share edges with Na2 bipyramid sites. Fe-containing octahedrons share corners with Na1 and Na3 sites share edges with Na2 sites. The Fe^{3+} ions site can be replaced by Eu^{3+} ions ions when Eu ions doping in the Na_3FeF_6 structure (Fig. 1a).

3.2 Characterization of the Na_3FeF_6

Fig. 2 shows the XRD patterns of sodium iron fluoride doped with Eu^{3+} at concentrations of 3%, 5%, 7%, 10%, and 15%. As concentration of the Eu ions increase from 3% to 7%, the diffraction peak gradually shifts to the left, diffraction angle θ decreases. According to the Bragg equation ($2d \sin\theta = n\lambda$), d increases with the decreasing of θ. The reason for this may be that as the concentration of Eu goes up, more Eu ions are incorporated into the Na_3FeF_6 lattice. Compared with Fe ions, Eu ions has a larger ionic radius. Therefore, the lattice constant would increase with the increase in the concentration of Eu ions in the lattice. The diffraction peaks of the Na_3FeF_6 with 5% Eu^{3+} doping are the highest, indicating the best crystallinity. The increase of Eu^{3+} concentration above 5% leads to growth of

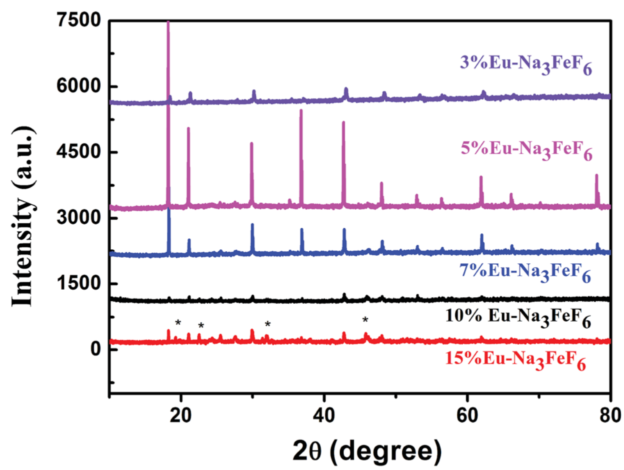

Fig. 2 X-ray diffraction patterns for samples of the Na_3FeF_6:Eu^{3+} with doping different concentrations of Eu^{3+}.

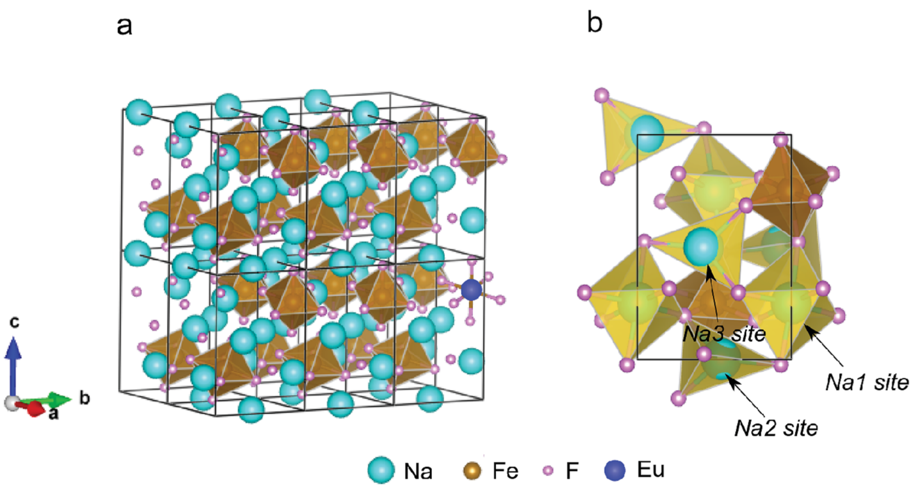

Fig. 1 (a) Crystal structure of Na_3FeF_6 projected along the *a* axis. (b) A detailed view of three different sodium sites in the Na_3FeF_6 crystal structure.

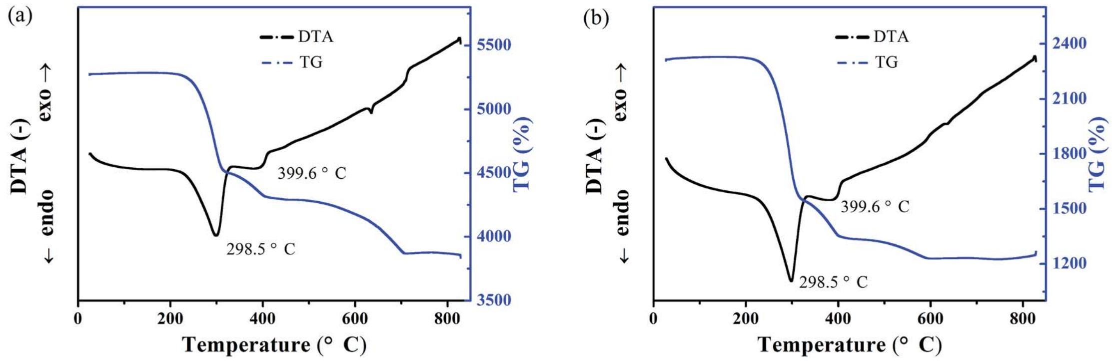

Fig. 3 TG and DTA curves: (a) Na_3FeF_6 and (b) Na_3FeF_6:5% Eu^{3+}.

lattice strain that prevents the further enhancement of crystallization. As can be seen from the XRD pattern, the solubility limit for Eu^{3+} ions in the lattice of Na_3FeF_6 is lower than 15%, at which considerable amount secondary phase appears due to the collapse of the lattice.[6] From the thermal analysis, the fluoride host Na_3FeF_6 is stable at temperatures up to around 255 °C. At higher temperatures, a strong endothermic peak appears accompanied with high weight loss in multiple stages, indicating the decomposition of the material (Fig. 3a). The detailed reactions involved in the decomposition remain to the unraveled. TG–TDA curver of Na_3FeF_6:5% Eu^{3+} is similarity with the pristine Na_3FeF_6 powder, indicating that the structure of the Na_3FeF_6 is stable when the 5% Eu^{3+} doping in Na_3FeF_6.

Fig. 4 and S2a† presents the typical SEM images of powders of Na_3FeF_6 doped with 5% Eu^{3+} and pristine Na_3FeF_6 powder. Octahedral particles are clearly observed, which is in accordance with the crystal structure of Na_3FeF_6 (Fig. 1), The average radius of these particles is around 4 μm and the surfaces of the particles are not smooth. The SEM image and the corresponding energy-dispersive spectrum EDS of the Na_3FeF_6:5% Eu (Fig. S1†) and pristine Na_3FeF_6 powder (Fig. S3†) shows elemental distribution of Na, Fe and F is revealed by elemental energy spectrum analysis and elemental Eu distribution in the Na_3FeF_6:5% Eu structure. Fig. S2b† shows the images of powders of Na_3FeF_6 doped with 15% Eu^{3+} including both octahedral particles and secondary phase with nanorod. The results in accordance with the XRD pattern from Na_3FeF_6:15% Eu. Fig. 4c–f show the SEM image and the corresponding EDS mapping images of Fe, Na, F and Eu elements. The result shows that all of the elements were detected and uniformly distributed.

3.3 Photoluminescence properties

Fig. 5 shows the absorption spectra of Na_3FeF_6 doped with different concentrations of Eu^{3+} (3%, 5%, 7%, 10%, 15% and

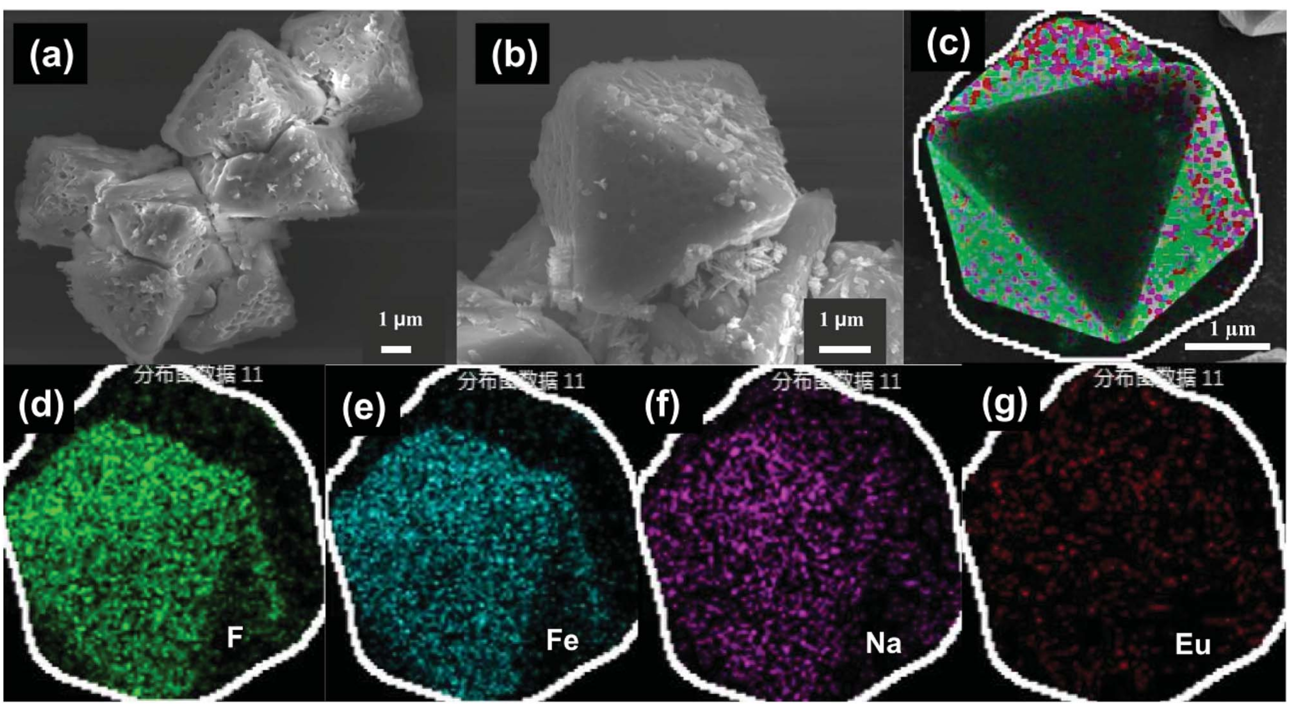

Fig. 4 SEM images image of the Na_3FeF_6:5% Eu^{3+} powders and the corresponding EDS mapping images of F, Fe, Na and Eu elements.

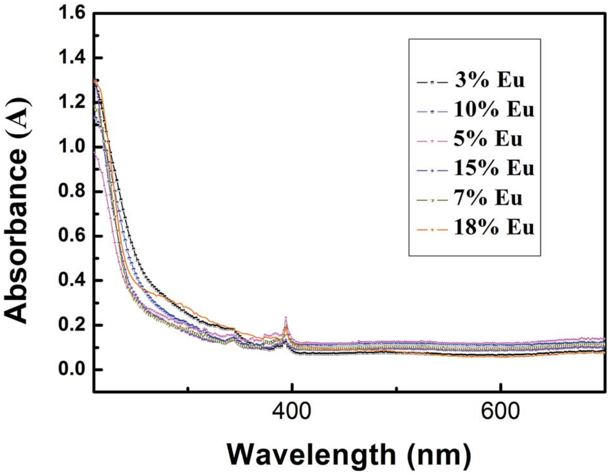

Fig. 5 Absorption spectra of the Na_3FeF_6 powder doped with different concentrations of Eu^{3+}.

18%) in the spectral range of 200–750 nm. It can be clearly seen that the Eu-doped Na_3FeF_6 powders exhibit obvious ultraviolet absorption at wavelength short than 300 nm. A small peak located at 395 nm can be attributed to the f–f transition of Eu^{3+}, while other transitions are not observed due to their weak transition probability. Obviously, the intensity of absorbance at 395 nm increases from 3% Eu to 5% Eu doped samples. At doping concentrations higher than 10%, the absorbance does not increase further, implying the doping limit of RE ions in the host of Na_3FeF_6.

As shown in Fig. 6a, the excitation spectra of 5% Eu^{3+} doped Na_3FeF_6 are measured at the wavelength of 615 nm. It can be observed from the excitation spectrum that there is a strong excitation band between 380–400 nm with a peak at around 395 nm, which can be well ascribed to the different f–f transitions of Eu^{3+}. Fig. 6b presents the emission spectra of Na_3FeF_6 doped with different concentrations of Eu^{3+} ions. The strongest emission peak is at 615 nm, which is attributed to the $^5D_0$–$^7F_2$ transitions of Eu^{3+}.[12] Increase of the Eu^{3+} doping level leads to the growth of emission intensity and the strongest intensity is observed for 5% Eu^{3+} doping. At doping levels higher than 5%, the emission intensity no longer increases due to concentration quenching. It is generally explained by the competition of two parallel processes: the emission process and the quenching process by self-absorption as well as cross-relaxation between Eu^{3+} ions.[7] At low Eu^{3+} doping concentrations, ion–ion interaction is negligibly small.[8] Above a certain Eu^{3+} concentration, the interactions between nearby Eu^{3+} ions becomes strong, which provides new energy dissipation pathways and reduces the rate of emission.[9]

Fig. 6c shows the emission spectra of the Na_3FeF_6:5% Eu^{3+} powders (the 5% Eu^{3+} doping Na_3FeF_6 was optimized from the Fig. 6b) synthesized at different temperatures. Under the excitation at 395 nm, the emission spectra show two peaks at 596 nm and 615 nm, respectively. The stronger peak at 615 nm

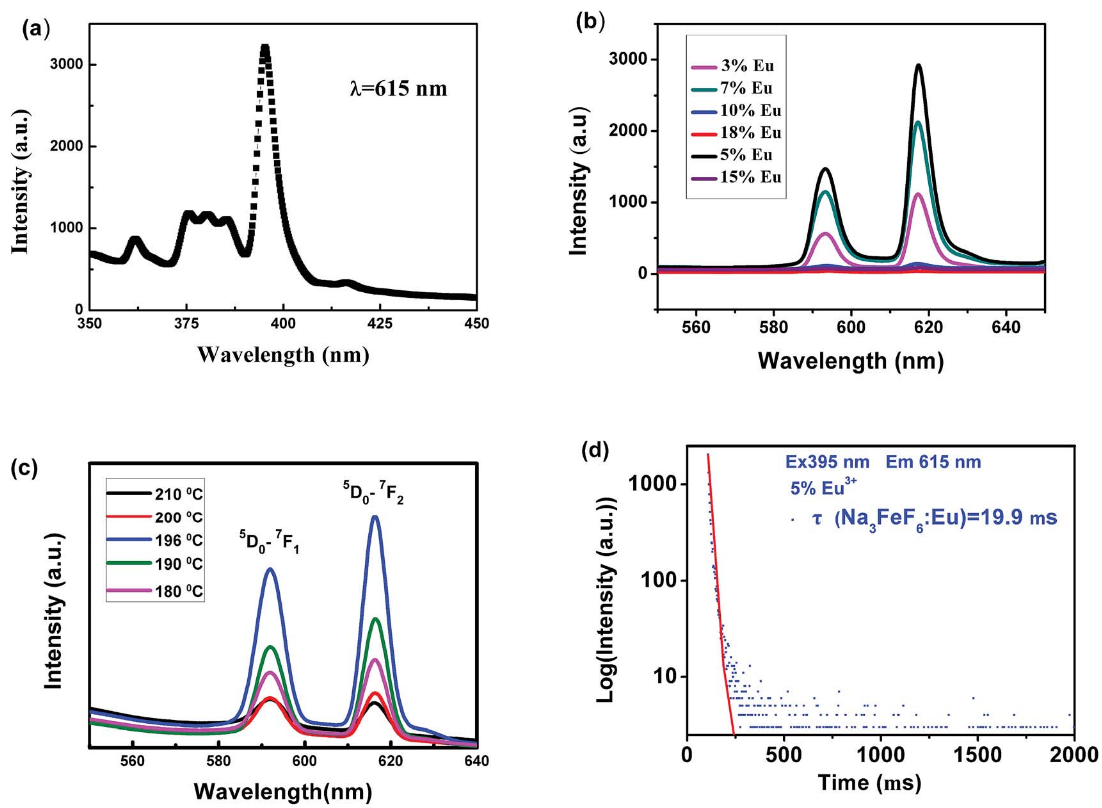

Fig. 6 (a) Excitation spectrum of Na_3FeF_6:5% Eu^{3+}. (b) Emission spectra of Na_3FeF_6 doped with different concentration of Eu^{3+}. (c) Emission spectra of the Na_3FeF_6:5% Eu^{3+} synthesized at different temperature. (d) Decay curves of the red (615 nm) emission under pulsed 395 nm excitation for the powder of Na_3FeF_6:5% Eu^{3+}.

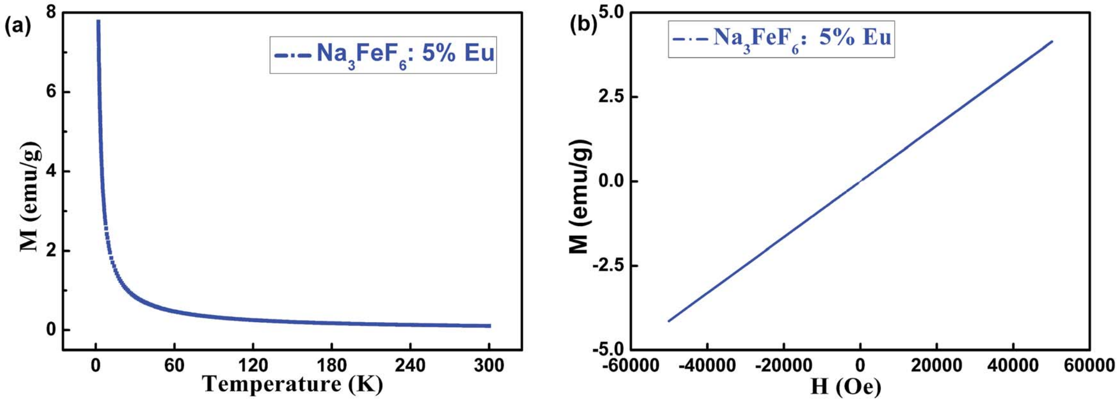

Fig. 7 The magnetization curve of Na_3FeF_6:5% Eu^{3+} particle at different temperature (a) and 300 K (b).

is due to the $^5D_0$–$^7F_2$ transition of the Eu ions and the other peak at 596 nm is owing to $^5D_0$–$^7F_1$ transition. The emission intensity is the highest for the sample obtained at 196 °C, and a higher synthesis temperature is not favorable for improving optical property. The decay curves of red (615 nm) emission was measured under pulsed 395 nm excitation (Fig. 6d). By fitting the decay curve with a bi-exponential decay function, we obtain a lifetime of 19.9 ms, which fall into the typical value for the red emission of Eu^{3+}.

The magnetization properties of Na_3FeF_6:5% Eu^{3+} particle was detected during warming up from 5 K to 300 K under field of 1000 Oe was applied. It was observed that the magnetization decrease rapidly from about 7.85 emu g^{-1} at 5 K to 0.4 emu g^{-1} at 60 K, then slowly decreasing with temperature increase from 60 K to 300 K (Fig. 7). The magnetization *versus* magnetic field (*M–H*) curves of Na_3FeF_6:5% Eu^{3+} particle by SQUID under the maximum magnetic field of 50 000 Oe at 300 K. It can be seen that the magnetization increase linearly from −4.15 emu g^{-1} to 4.14 emu g^{-1} under magnetic field from −50 000 Oe to 5000 Oe. The results considered that Na_3FeF_6:5% Eu^{3+} is paramagnetic material. Fig. S5† shows the magnetization curves of Na_3FeF_6 doped with different concentration of Eu^{3+} ions at 300 K. Increase of the Eu^{3+} doping level leads to the decrease of paramagnetic intensity, it maybe due to the higher paramagnetic intensity from Fe^{3+} ions compare with Eu^{3+} ions and the positions of Fe^{3+} ions in Na_3FeF_6 structure were gradually replaced by the Eu^{3+} ions.

4. Conclusions

The phosphor powder of Na_3FeF_6:Eu is prepared by hydrothermal method. The structures of the Na_3FeF_6:Eu powders were characterized by X-ray diffraction (XRD) and SEM. Octahedral particles with homogeneous surfaces are obtained. Optical measurement indicates that Na_3FeF_6 doped with 5% Eu^{3+} and synthesized at the temperature of 196 °C shows the strongest emission intensity. The magnetization of Na_3FeF_6:5% Eu^{3+} decrease rapidly from about 7.85 emu g^{-1} at 5 K to 0.4 emu g^{-1} at 60 K, then slowly decreasing with temperature increase from 60 K to 300 K. The results pave the way for the study of the magneto-optical effect in this material.

Conflicts of interest

There are no conflicts to declare.

Acknowledgements

This work was financially supported by the National Key R&D Program of China (Grant No. 2018YFB1107200), the National Natural Science Foundation of China (Grant No. 61404071, 61575091, 61675094, 51132004, 51072054, 51102209, 51472091, 51772270 and 51471082), Key projects of Henan Provincial Education Department (No. 16A140029 and No. 14B40010), the National Basic Research Program of China (2011CB808100), the Natural Science Foundation of Henan Province of China (162300410201), the Henan Provincial Department of Science and Technology Research Project (162102210303), the Fundamental and Cutting-edge Technology Research Program of Henan Province (152300410218), the Key Scientific Research Projects of Henan Province (Grants 16A140014 and 16A140016), the Program for Young Teachers of Higher School in Henan Province (2013GGJS-153), the Program for Innovation Talents (in Science and Technology) in University of Henan Province (16HASTIT044), Youth Backbone Teacher Training Program in Henan province (2017GGJS137) Open funds of State Key Laboratory of Precision Spectroscopy, East China Normal University and State Key Laboratory of High Field Laser Physics, Shanghai Institute of Optics and Fine Mechanics, Chinese Academy of Sciences.

References

1 H. Yun, M. S. Ahmed, K. Lee, S. Jeon and C. W. Lee, Potential enhancement of antibacterial activity of graphene oxide-silver nanocomposite by introducing C_2 carbon chain linkage, *Appl. Surf. Sci.*, 2016, **360**, 915–920.
2 H. Jia, Z. Chen, Z. L. Liu, J. G. Zhao, C. L. Ding, H. F. Yang, W. Y. Zhang, X. F. Liu and J. R. Qiu, CaF_2:Eu films shine novel blue, white or red luminescence though adjustment of the valence state of Eu ions using the electro-deposition method, *J. Mater. Chem. C*, 2017, **5**, 12085–12089.

3 X. W. Zhang, Y. Y. Liu, J. Gao, G. S. Han, M. F. Hu, X. L. Wu, H. Q. Cao, X. Y. Wang and B. J. Li, Defect-rich (Co-CoS_2) x@Co_9S_8 nanosheets derived from monomolecular precursor pyrolysis with excellent catalytic activity for hydrogen evolution reaction, *J. Mater. Chem. A*, 2018, **6**, 7977–7987.

4 N. N. Sulaiman, N. S. Mustafa and M. Ismail, Effect of Na_3FeF_6 catalyst on the hydrogen storage properties of MgH_2, *Dalton Trans.*, 2016, **45**, 7085–7093.

5 H. Q. Wang, M. Batentschuk, A. Osvet, L. Pinna and C. J. S. Brabec, Rare-earth ion doped up-conversion materials for photovoltaic applications, *Adv. Mater.*, 2011, **23**, 2675–2680.

6 S. Güner, M. Amir, M. Geleri, M. Sertkol and A. Baykal, Magneto-optical Properties Mn^{3+} substituted Fe_3O_4 nanoparticles, *Ceram. Int.*, 2018, **11**, 324–329.

7 A. Mehta, T. Thundat, M. D. Barnes, V. Chhabra, R. Bhargava, A. P. Bartko and R. M. Dickson, Size-correlated spectroscopy and imaging of rare-earth-doped nanocrystals, *Appl. Opt.*, 2003, **42**, 2132–2139.

8 T. H. Shin, Y. Choi, S. Kim and S. J. Cheon, Recent advances in magnetic nanoparticle-based multi-modal imaging, *Chem. Soc. Rev.*, 2015, **44**, 4501–4516.

9 L. Zeng, L. Luo, Y. Pang, S. Luo, G. Lu and A. Wu, *In vivo* targeted magnetic resonance imaging and visualized photodynamic therapy in deep-tissue cancers using folic acid-functionalized superparamagnetic upconversion nanocomposites, *Nanoscale*, 2015, **7**, 8946–8954.

10 M. L. Zhang, Z. G. Xia and Q. L. Liu, Thermally stable $K_xCs_{1-x}AlSi_2O_6$:Eu^{2+} phosphors and their photoluminescence tuning, *J. Mater. Chem. C*, 2017, **5**, 7489–7494.

11 T. Guo, Y. Lin, W. J. Zhang, J. S. Hong, R. H. Lin, X. P. Wu, C. H. Lu and H. H. Yang, High-efficiency X-ray luminescence in Eu^{3+}-activated tungstate nanoprobes for optical imaging through energy transfer sensitization, *Nanoscale*, 2018, **10**, 1607–1612.

12 M. J. Zhong, M. P. Hedges, R. L. Ahlefeldt, J. G. Bartholomew, S. E. Beavan, S. M. Wittig, J. J. Longdell and M. J. Sellars, Optically addressable nuclear spins in a solid with a six-hour coherence time, *Nature*, 2015, **517**, 177–180.

13 D. Q. Chen, Z. Y. Wan, X. Chen, Y. J. Yuan and J. S. Zhong, Large-scale room-temperature synthesis and optical properties of perovskite related Cs_4PbBr_6 fluorophores, *J. Mater. Chem. C*, 2016, **4**, 10646–10653.

14 J. J. H. A. VanHest, G. A. Blab, H. C. Gerritsen, G. D. M. Donega and A. Meijerink, Probing the Influence of Disorder on Lanthanide Luminescence Using Eu-Doped $LaPO_4$ Nanoparticles, *J. Phys. Chem. C*, 2017, **121**, 19373–19382.

15 H. X. Peng, B. Cui, G. M. Li, Y. S. Wang, N. N. Li, Z. G. Chang and Y. Y. Wang, A multifunctional β-CD-modified Fe_3O_4@ZnO:Er^{3+}, Yb^{3+} nanocarrier for antitumor drug delivery and microwave-triggered drug release, *Mater. Sci. Eng., C*, 2015, **46**, 253–263.

16 D. Q. Chen, W. W. Wu, Y. J. Yuan, Y. Zhou, Z. Y. Wan and P. Huang, Intense multi-state visible absorption and full-color luminescence of nitrogen-doped carbon quantum dots for blue-light-excitable solid-state-lighting, *J. Mater. Chem. C*, 2016, **4**, 9027–9035.

17 J. Q. Wan, Q. Liu, G. H. Liu, Z. Z. Zhou, J. Ni and R. J. Xie, A novel Eu^{2+} activated G-$La_2Si_2O_7$ phosphor for white LEDs: SiC-reduction synthesis, tunable luminescence and good thermal stability, *J. Mater. Chem. C*, 2017, **5**, 1614–1623.

18 Q. L. Ma, J. X. Wang, X. T. Dong, W. S. Yu and G. X. Liu, Magnetic-upconversion luminescent bifunctional flexible coaxial nanoribbon and Janus nanoribbon: one-pot electrospinning preparation, structure and enhanced upconversion luminescent characteristics, *Chem. Eng. J.*, 2015, **260**, 222–230.

19 G. F. Wang, Q. Peng and Y. D. Li, Lanthanide-doped nanocrystals: synthesis, optical-magnetic properties, and applications, *Acc. Chem. Res.*, 2011, **44**, 322–332.

20 V. Shanmugam, S. Selvakumar and C. S. Yeh, Near-infrared light-responsive nanomaterials in cancer therapeutics, *Chem. Soc. Rev.*, 2014, **43**, 6254–6287.

21 A. Kumar, A. Kumar, G. Sharma, A. H. Al-muhtaseb, M. Naushad, A. A. Ghfar and F. J. Stadler, Quaternary magnetic BiOCl/g-C_3N_4/Cu_2O/Fe_3O_4 nano-junction for visible light and solar powered degradation of sulfamethoxazole from aqueous environment, *Chem. Eng. J.*, 2018, **334**, 462–478.

22 S. Y. Yu, X. C. Gao, H. Jing, R. H. Zhang, X. L. Gao and H. Q. Su, Fabrication and characterization of novel magnetic/luminescent multifunctional nanocomposites for controlled drug release, *CrystEngComm*, 2014, **16**, 6645–6653.

23 H. Wang, Z. Y. Wei, H. Matsui and S. Q. Zhou, Fe_3O_4/carbon quantum dots hybrid nanoflowers for highly active and recyclable visible-light driven photocatalyst, *J. Mater. Chem. A*, 2014, **2**, 15740–15745.

24 H. R. Yin, Y. Gao, R. Buchanan, J. B. Song and M. Y. Li, Wavelength dependence of Tb^{3+} doped magneto-optical glass Verdet constant, *Ceram. Int.*, 2018, **44**, 10929–10933.

25 L. Wang and Y. D. Li, $Na(Y_{1.5}Na_{0.5})F_6$ Single-Crystal Nanorods as Multicolor Luminescent Materials, *Nano Lett.*, 2006, **6**, 1645–1649.

26 K. He, Y. N. Zhou, P. Gao, L. P. Wang, N. Pereira, G. G. Amatucci, K. W. Nam, X. Q. Yang, Y. M. Zhu, F. Wang and D. Su, Sodiation *via* Heterogeneous Disproportionation in FeF_2 Electrodes for Sodium-Ion Batteries, *ACS Nano*, 2014, **8**, 7251–7259.

27 E. H. Song, J. Q. Wang, S. Ye, X. F. Jiang, M. Y. Peng and Q. Y. Zhang, Room-temperature synthesis and warm-white LED applications of Mn^{4+} ion doped fluoroaluminate red phosphor Na_3AlF_6:Mn^{4+}, *J. Mater. Chem. C*, 2016, **4**, 2480–2487.

28 G. Brunton, The crystal structure of Na_3CrF_6, *Mater. Res. Bull.*, 1969, **4**, 621–626.